Rational Design of the Pore System within the Framework Aluminium Alkylenediphosphonate Series

Howard G. Harvey,[a] Ben Slater,[a] and Martin P. Attfield*[b]

Abstract: We report here on the solvothermal synthesis and crystal structure of the hybrid organic–inorganic framework material $Al_2[O_3PC_3H_6PO_3](H_2O)_2F_2{\cdot}H_2O$ (orthorhombic, *Pmmn*, $a = 12.0591(2)$ Å, $b = 19.1647(5)$ Å, $c = 4.91142(7)$ Å, $Z = 4$), the second member of the $Al_2[O_3PC_nH_{2n}PO_3](H_2O)_2F_2{\cdot}H_2O$ series. The structure consists of corrugated chains of corner-sharing AlO_4F_2 octahedra in which alternating AlO_4F_2 octahedra contain two fluorine atoms in a *trans* or a *cis* configuration. The diphosphonate groups link the chains together through Al–O–P–O–Al bridges and through the propylene groups to form a three-dimensional framework structure containing a one-dimensional channel system. The linkage of the corrugated inorganic Al–O–P layers within the structure results in the formation of two types of channel that differ in size, shape and composition. The smaller channel is unoccupied; the larger channel is more elongated and contains two extra-framework water molecules per unit cell. A computational investigation into the driving force that controls the stacking arrangement of the Al–O–P inorganic layers within this series of compounds reveals that the stacking is found to be controlled by thermodynamic factors, arising chiefly from the conformation of the organic linker molecule used to connect the inorganic sheets. It is found that the registration of the inorganic layers can be engineered by selecting an appropriate, simple organic spacer or linker alkyl chain, where an even number of carbon atoms in the alkyl chain directs formation of aligned, stacked, inorganic sheets (AAAAAA), and an odd number directs formation of unaligned, stacked sheets (ABABAB) and the formation of one or two channel types in the resultant structure, respectively. This combination of alkyl-chain linkers in conjunction with corrugated inorganic layers is an effective tool to rationally design the pore system of hybrid framework materials.

Keywords: aluminium · density functional · microporous materials · organic–inorganic hybrid composites · solid-state structures

Introduction

Great interest is currently being shown in the family of organic–inorganic hybrid framework materials on account of their novel properties and the potential for rational design of their structure and functionality.[1,2] This interest is fuelled by the enduring desire to synthesise extended crystalline solid-state materials in a systematic manner to allow the type of precision over the dimensions and functionality of the material that is already practiced in synthetic organic chemistry. Such an approach has been demonstrated, in an exemplary fashion, by Yaghi and co-workers in their formation of a series of isoreticular metal-organic frameworks constructed from octahedral Zn–O–C clusters and an array of 16 different types of organic linkers that bridge these clusters.[3,4] The linkers inserted into the structure included those of similar size, but different functionality, and those that expand the pore dimensions of the materials. It is found that rigid linker groups, for instance, the phenyl group, are needed to maintain the structure of these frameworks. However, the necessity to include such rigid groups in the linker makes it synthetically more complex to produce linkers that are longer by small incremental amounts, for instance, inserting one C atom, as opposed to the use of alkyl chains where it is facile to produce chains that are one -CH_2- group longer. In this work, we show and explain how the use of simple alkyl chain linkers in conjunction with corrugated inorganic layers can be used to rationally design the number

[a] Dr. H. G. Harvey, Dr. B. Slater
Davy–Faraday Research Laboratory
The Royal Institution of Great Britain
21 Albemarle Street, London, W1S 4BS (UK)

[b] Dr. M. P. Attfield
UMIST Centre for Microporous Materials
Department of Chemistry, UMIST
PO Box 88, Manchester, M60 1QD (UK)
Fax: (+44) 161-200-4559
E-mail: m.attfield@umist.ac.uk

Supporting information for this article is available on the WWW under http://www.chemeurj.org/ or from the author. The Supporting Information includes the ^{31}P and ^{19}F MAS solid-state NMR spectra for $Al_2[O_3PC_3H_6PO_3](H_2O)_2F_2{\cdot}H_2O$.

DOI: 10.1002/chem.200400078

of channel types, and their height, within the resultant hybrid framework materials. This methodology provides a powerful element to the rational design of framework solids and their micropore volume.

If simple alkyl groups are used as linkers in these hybrid materials, it is desirable for the inorganic fragments to have a greater structural integrity, as is found in infinite chains[5] or planes.[6] However, there are relatively few examples of crystalline hybrid compounds in which the inorganic fragment maintains an identical form in a series of compounds in which the length of the alkyl chain linker increases in incremental steps. Two systems reported by Férey and co-workers exhibit this property. They are both based on chains of edge-sharing rare-earth polyhedra. One system is the rare-earth dicarboxylates, $[Pr(H_2O)]_2[O_2C(CH_2)_2CO_2]_3{\cdot}H_2O$ and $[Pr(H_2O)]_2[O_2C(CH_2)_3CO_2]_3{\cdot}4\,H_2O$, in which the Ln–O–C chains are joined in two directions by the linkers of the dicarboxylate groups to form a three-dimensional network containing channels in a direction parallel to the chains.[7,8] The other system is the rare-earth diphosphonates $LnH[O_3P(CH_2)_nPO_3]$ ($n = 1, 2, 3$), which also contain chains of edge-sharing rare-earth polyhedra linked together by the -PO_3 groups of the diphosphonate species to form Ln–O–P layers that are connected in one direction by the alkyl group linkers of the diphosphonate moiety.[9] These materials are also three-dimensional networks containing empty channels in one direction. Clearfield and co-workers have produced a series of copper alkylenediphosphonates,[10,11] $Cu_2[(O_3P(CH_2)_2PO_3)(H_2O)_2]$, $Cu_2[(O_3P(CH_2)_3PO_3)(H_2O)_2]{\cdot}H_2O$, $Cu_2[(O_3P(CH_2)_4PO_3)(H_2O)_2]{\cdot}2\,H_2O$ and $Cu_2[(O_3P(CH_2)_5PO_3)(H_2O)_2]{\cdot}2.8\,H_2O$ that all contain chains of Cu polyhedra linked together by the -PO_3 groups of the diphosphonate species to form Cu–O–P layers that are joined in one direction by the alkyl group linkers of the diphosphonate group. The structure of the Cu–O–P layer of the $n = 2,3$ members is different to that of the $n = 4,5$ members. The size of the channels in all these Ln and Cu series increase as the length of the alkyl-group linker increases. This is confirmed by the water content of the copper diphosphonate compounds increasing as the alkyl chain length, and thus the channel size, increases within them. The inorganic chains or layers in the aforementioned materials are all essentially linear so that the number of differently shaped channels in these materials is one. If the inorganic layers of the hybrid material are themselves nonlinear, for example corrugated, it is possible to form materials with either one type of channel or with two if such layers are linked together so that the inorganic corrugated layers are either aligned (in-phase) with an AAAAAA stacking arrangement or unaligned (out-of-phase) with an ABABAB stacking arrangement (Figure 1). An example of the latter arrangement is found in the structure of $Zn_2[(HO_3P(CH_2)_3PO_3)_2]{\cdot}2\,H_2O$ that contains elliptical and circular parallel, unidimensional tunnels.[12] Control of the stacking arrangement of the constituent corrugated layers in lamellar materials is known and can be controlled by the use of organic ammonium cations as structure-directing agents.[13,14] Control of the alignment of the corrugated inorganic chains or layers, through a suitable choice of the nature of the organic linker, would determine the number of types of channel, and their size, in the resultant framework material, and provides a new element for the rational design of the pore system of such hybrid materials.

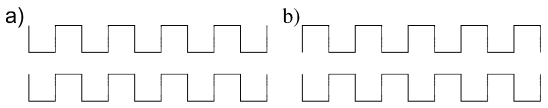

Figure 1. A schematic illustrating the formation of different channel types in structures by arrangement of corrugated layers in a) an aligned fashion to give one type of channel, and b) an unaligned fashion to give two types of channel.

We recently reported the synthesis and structure of the first aluminium diphosphonate material, $Al_2[O_3PC_2H_4PO_3](H_2O)_2F_2{\cdot}H_2O$, a framework structure containing a one-dimensional channel system with one crystallographic species of extra-framework molecule occupying the channels.[15,16] Subsequent research into this system has yielded the $n = 3$ member of the series $Al_2[O_3PC_nH_{2n}PO_3](H_2O)_2F_2{\cdot}H_2O$, for which we have reported preliminary unit cell and symmetry information.[17] Herein, we describe the full synthesis, crystal structure and properties of $Al_2[O_3PC_3H_6PO_3](H_2O)_2F_2{\cdot}H_2O$ as well as the use of computational methods to explain how the number of channel types and linkage of the inorganic layers is controlled by the alkyl chain linker in the $n = 2,3$ members of this series and also to predict the form of the structure of the $n = 4$ member.

Experimental and Computational Sections

Synthesis: All reagents and solvents were obtained from Aldrich, with the exception of propylenediphosphonic acid (Alfa-Aesar), and were used without further purification. Initial synthesis of $Al_2[O_3PC_3H_6PO_3](H_2O)_2F_2{\cdot}H_2O$ was accomplished by mixing $Al_2(SO_4)_3{\cdot}18\,H_2O$ (2.360 g), $H_2O_3PC_3H_6PO_3H_2$ (1.489 g), HF/pyridine (70 wt% HF, 0.415 g), pyridine (7.110 g) and de-ionized water (4.350 g) to form a reagent mixture that was loaded into a 23-mL Teflon-lined steel autoclave and heated for five days at 160 °C. The product mixture was slowly cooled to room temperature. The polycrystalline product was separated by suction filtration, washed and dried at room temperature. The polycrystalline product was also synthesised from an initial synthesis gel composition of $Al_2(SO_4)_3{\cdot}18\,H_2O$ (1.573 g), $H_2O_3PC_3H_6PO_3H_2$ (0.987 g), HF/pyridine (70 wt% HF, 0.415 g), pyridine (7.110 g) and de-ionized water (4.350 g). The mixture was heated at 190 °C for 12 days. Microprobe analysis of the samples indicated an Al:P ratio of 1:1 and that fluorine was present in the material.

NMR spectroscopic measurements: All magic-angle spinning solid-state nuclear magnetic resonance (MAS SS NMR) spectra were recorded on a Bruker MSL300 spectrometer. The ^{31}P spectrum was recorded with a 85% solution of H_3PO_4 as the reference with the spectrometer operating at a frequency of 121.495 MHz, with recycle delays of 60 s and sample spinning speeds of 7 kHz. The spectrum collected for the ^{19}F nuclei were referenced to $CFCl_3$ with the spectrometer operating at a frequency of 282.4 MHz, recycle delays of 5 s and a sample spinning speed of 4.3 kHz.

Thermogravimetric analysis: Thermogravimetric analysis data (TGA) were collected with a Shimadzu TGA50 thermogravimetric analyser. The sample was heated in an alumina crucible under flowing nitrogen gas from 25 to 900 °C at a heating rate of 5 °C min^{-1}.

Ab initio powder-structure solution: The X-ray data used to determine the unit cell parameters of $Al_2[O_3PC_3H_6PO_3](H_2O)_2F_2{\cdot}H_2O$ were collected during a 12 h scan on a laboratory Siemens D500 X-ray diffractometer employing Ge-monochromated $Cu_{K\alpha1}$ radiation. The first 20 low-angle

Bragg reflections were used to determine the orthorhombic unit cell parameters of the material with the auto-indexing program LZON[18] contained within the CRYSFIRE suite of indexing programs.[19] Synchrotron X-ray data were collected on a sample contained in a 0.5 mm diameter Lindemann glass capillary tube mounted on the high-resolution X-ray diffractometer at station 2.3, CCLRC Synchrotron Radiation Source (Daresbury, UK). The incident X-ray wavelength was 1.300188 Å, selected with a Si(111) monochromator. The capillary tube was spun during data collection to minimise preferred orientation and sampling effects. Data were collected in steps of 0.01° in 2θ for a total of 17 h, with a collection time per step of 4 s between 3.5 and 20° 2θ, 6 s between 20 and 50° 2θ, 11 s between 50 and 72° 2θ and 15 s between 72 and 80° 2θ. Corrections were made for the decay of the synchrotron beam intensity by comparison with a beam-flux monitor.

Inspection of the synchrotron X-ray diffraction pattern revealed systematic absences consistent with the space group $P22_12_1$. Observed structure factors were extracted from this diffraction data by the Le Bail method,[20] as implemented in the GSAS suite of programs.[21] The background of the diffraction profile was fitted with a Cosine Fourier series running through 66 fixed points in the profile. The peak profiles were described by a pseudo-Voigt function with additional terms used to account for anisotropic particle-size and strain-broadening effects. The extracted structure factors were used in the direct methods program SIRPOW 97,[22] by using the EXPO interface,[23] to provide the Al, P and some of the O and C atoms of the structure. This output was used as the starting model for the Rietveld refinement, again using the GSAS suite of programs.[21] The remaining atoms of the structure were located from difference Fourier maps. Inspection of the structure with the Addsym program, within the PLATON suite of programs,[24] revealed the structure to have the higher symmetry of *Pmmn*. This structure was identical to that solved in $P22_12_1$, but contained single crystallographically independent phosphorus and fluorine atoms, three fewer oxygen atoms and one fewer carbon atom in the asymmetric unit. The structure was refined twice using each of the space groups following the same procedure. Initially, soft constraints were applied to the Al–O/F, P–O/C and C–C distances within the structure, with the soft constraint weighting factor fixed at a high value. As the refinement progressed, the soft constraint weighting factor was reduced to a final value of one in the latter cycles of the refinement. The final cycle of least-squares refinement included the background coefficients, peak profile parameters as well as the positional and isotropic displacement parameters for all atoms in the structure. The thermal parameters of the Al and P atoms as well as the O, F and C atoms were constrained to have the same value during refinement. The Rietveld refinement gave reasonable bond lengths, angles and residuals in both symmetries; however, the higher symmetry solution, *Pmmn*, is reported because this fit was obtained from fewer refineable parameters. The crystallographic data and structure refinement parameters are given in Table 1. Atomic coordinates and isotropic displacement parameters are provided in Table 2. Selected bond lengths and angles are presented in Table 3. The final observed, calculated and difference profiles are plotted in Figure 2, and the asymmetric unit is shown in Figure 3.

Table 1. Crystal data and structure refinement parameters for $Al_2[O_3PC_3H_6PO_3](H_2O)_2F_2{\cdot}H_2O$.

formula	$Al_2P_2F_2O_9C_3H_{12}$
formula weight	346.93
T[K]	293
λ[Å]	1.300188
space group	*Pmmn*
a[Å]	12.0591(2)
b[Å]	19.1647(5)
c[Å]	4.91142(7)
V[Å^3]	1135.07(5)
Z	4
ρcalcd[g cm^{-3}]	1.954
no. of reflections	628
no. of fitted parameters	48
R_p	0.0645
R_{wp}	0.0787
R_F	0.0789
χ^2	1.363

Table 2. Atomic coordinates and isotropic thermal displacement parameters[Å^2] for $Al_2[O_3PC_3H_6PO_3](H_2O)_2F_2{\cdot}H_2O$.

Atom	x	y	z	U_{iso}
Al1	0.0000	0.0000	0.0000	0.0073(6)
Al2	0.2500	0.0623(3)	0.734(1)	0.0073(6)
P1	0.0154(3)	0.1047(2)	0.5024(8)	0.0073(6)
O1	0.030(6)	0.0853(3)	0.200(1)	0.015(1)
O2	0.1424(4)	0.1102(4)	0.534(2)	0.015(1)
O3	−0.0413(5)	0.0492(4)	0.683(1)	0.015(1)
O4	0.2500	−0.0128(5)	0.468(2)	0.015(1)
O5	0.2500	0.1319(5)	0.043(2)	0.015(1)
O6[a]	0.6927(9)	0.1444(6)	0.087(2)	0.015(1)
F1	0.1461(4)	0.0135(3)	0.926(1)	0.015(1)
C1	−0.0516(7)	0.1876(3)	0.559(2)	0.015(1)
C2	0.012(1)	0.2500	0.451(3)	0.015(1)

[a] Occupancy for O6 = 0.5

CCDC-229316 contains the supplementary crystallographic data for this paper. These data can be obtained free of charge via www.ccdc.cam.ac.uk/conts/retrieving.html (or from the Cambridge Crystallographic Data Centre, 12 Union Road, Cambridge CB21EZ, UK; fax: (+44) 1223-336033; or deposit@ccdc.cam.uk).

Table 3. Selected bond lengths[Å] and angles[°] for $Al_2[O_3PC_3H_6PO_3](H_2O)_2F_2{\cdot}H_2O$.

Al1–F1[a]	1.817(4)	Al2–F1	1.828(5)
Al1–F1[b]	1.817(4)	Al2–F1[d]	1.828(5)
Al1–O1	1.909(5)	Al2–O2	1.866(5)
Al1–O1[c]	1.909(5)	Al2–O2[d]	1.866(5)
Al1–O3[a]	1.888(5)	Al2–O4	1.944(8)
Al1–O3[b]	1.888(5)	Al2–O5[e]	2.022(8)
P1–O1	1.537(5)	P1–C1	1.804(6)
P1–O2	1.543(5)	P1–O3	1.544(6)
C1–C2	1.519(8)		
F1[a]-Al1-F1[b]	180.0	F1-Al2-F1[d]	86.6(4)
F1[a]Al1-O1	87.9(3)	F1-Al2-O2	92.6(2)
F1[a]-Al1-O1[c]	92.2(3)	F1-Al2-O2[d]	178.6(5)
F1[a]-Al1-O3[a]	91.1(2)	F1-Al2-O4	88.2(4)
F1[a]-Al1-O3[b]	88.9(2)	F1-Al2-O5[e]	87.0(4)
F1[b]-Al1-O1	92.2(3)	F1[d]Al2-O2	178.6(5)
F1[b]-Al1-O1[c]	87.9(3)	F1[d]-Al2-O2[d]	92.6(2)
F1[b]-Al1-O3[a]	88.9(2)	F1[d]-Al2-O4	88.2(4)
F1[b]-Al1-O3[b]	91.1(2)	F1[d]-Al2-O5[e]	87.0(4)
O1-Al1-O1[c]	180.0(2)	O2-Al2-O2[d]	88.1(5)
O1-Al1-O3[a]	90.2(3)	O2-Al2-O4	90.6(4)
O1-Al1-O3[b]	89.9(3)	O2-Al2-O5[e]	94.1(4)
O1[c]-Al1-O3[a]	89.9(2)	O2[d]-Al2-O4	90.6(4)
O1[c]-Al1-O3[b]	90.1(2)	O2[d]-Al2-O5[e]	94.1(4)
O3[a]-Al1-O3[b]	180.0	O4-Al2-O5[e]	173.5(6)
O1-P1-O2	102.2(5)	O2-P1-O3	115.3(4)
O1-P1-O3	110.1(4)	O2-P1-C1	111.7(4)
O1-P1-C1	108.6(4)	O3-P1-C1	108.6(4)
C1-C2-C1[f]	103.9(9)	P1-C1-C2	114.3(6)

Symmetry transformations used to generate equivalent atoms: a: x, y, $z-1$; b: $-x$, $-y$, $-z+1$; c: $-x$, $-y$, $-z$; d: $0.5-x$, y, z; e: x, y, $z+1$; f: x, $0.5-y$, z

Structure and energetics analysis using computational methods: The purpose of undertaking a computational study of the diphosphonate family was primarily motivated by a desire to understand how the stacking sequence observed in these materials is dictated by the flexibility or rigidity of each component of the cell. The hybrid nature of these materials suggests that the structure-directing properties of each component (inorganic or organic) of the cell will be different. Specifically, we expect that the

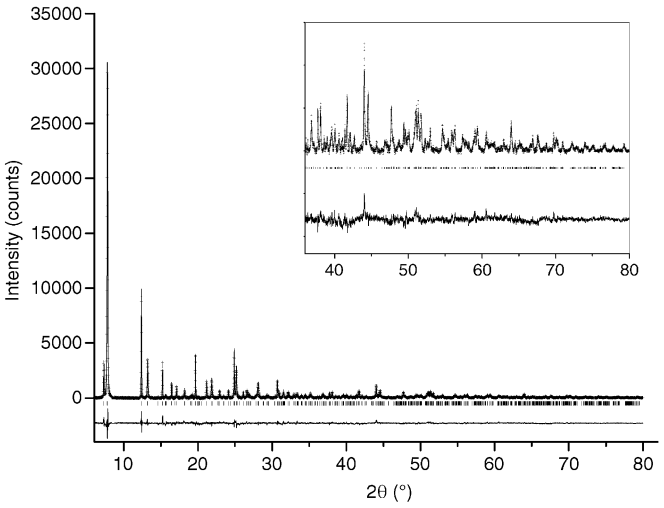

Figure 2. The final observed (+), calculated (——) and difference plots for the Rietveld refinement of $Al_2[O_3PC_3H_6PO_3](H_2O)_2F_2{\cdot}H_2O$. The tick marks are calculated 2θ angles for the Bragg peaks.

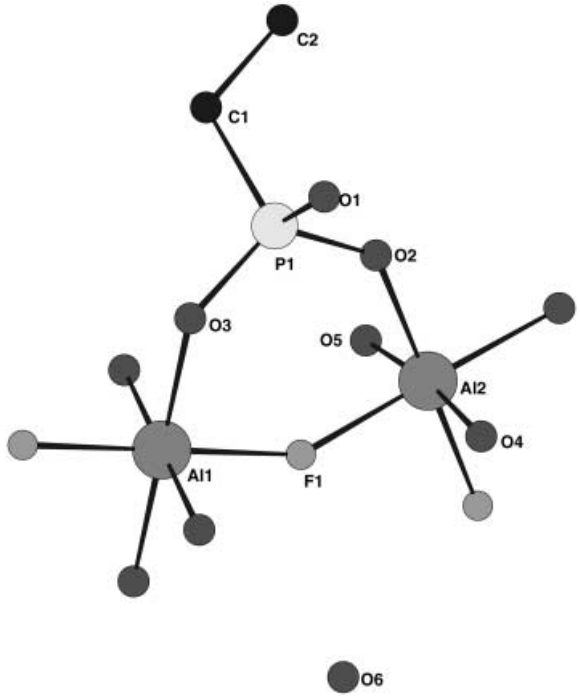

Figure 3. The asymmetric unit of $Al_2[O_3PC_3H_6PO_3](H_2O)_2F_2{\cdot}H_2O$ (labelled atoms) with the full first coordination sphere of the Al and P atoms included for clarity.

organic component of the cell will have a higher conformational freedom than the inorganic part, and, in simple chemical terms, we expect the organic part to be flexible and the inorganic part to be relatively rigid. However, there are two further elements to this stacking problem: 1) there will be a preferred stacking arrangement of the inorganic layers, which will be dictated by the long-ranged coulombic and van der Waals energy, and 2) the connection between the organic linker and the inorganic layer will be influenced by the conformations the linker can adopt at a given temperature.

To assess the validity of these simple chemical assertions, first-principles computational methods were used to probe the relative energies of topologically related structures formed by using alkylenediphosphonic acids of different length, to rationalise the driving forces that govern the preferred formation of one structure over another. Plane-wave based, density functional theory (DFT) was selected as the tool to accurately calculate the energy and geometry of the structures. The choice of using a DFT-based method, in contrast to a classical forcefield approach, was motivated by two factors: 1) The hybrid nature of these novel materials provides a challenge to existing forcefields because the link between the inorganic and organic component is not well-parameterised. 2) To analyse the driving force of stacking, the energy difference between two phases was carried out together with a deconvolution of the cell constituents. Breaking bonds within the cell would stretch the capabilities of the classical approach because this process is not inherently well-described by simple harmonic or Morse-type energy functions and has to be carefully parameterised. Ironically, the parameterisation of the bond-breaking process is often achieved by fitting against high-quality electronic structure calculations. Clearly, in this instance, the parameterisation would be self-defeating and involve a doubling of the computational effort.

Ultrasoft pseudo-potentials were used to describe the core states of the atoms with a kinetic energy cut-off of 380 eV. The PW91 exchange correlation recipe[25] was used throughout this work within the GGA formalism. *K*-point sampling was performed on a single Γ point in the full unit cell. Because these materials are relatively porous and are of an insulating nature, more frequent sampling of the electron density does not change the total energy, and hence this approximation is a reasonable one. Additionally, the cell dimensions are large enough for the total energy to be invariant with more frequent *k*-point sampling. All calculations were undertaken with the CASTEP code,[26] and geometry optimisation was carried out so that the forces on the atoms were less than 0.005 eV $Å^{-1}$ and the stress within the unit cell was eliminated.

The initial structures to be optimised were generated from the observed crystal structures of $Al_2[O_3PC_2H_4PO_3](H_2O)_2F_2{\cdot}H_2O$[15] and the structure of $Al_2[O_2PC_3H_6PO_3](H_2O)_2F_2{\cdot}H_2O$ reported herein. The positions of hydrogen atoms within the cell have not been determined experimentally, and therefore, for both carbon and water oxygen atoms, chemical intuition was used to provide an initial model. This model was then partially refined by optimising the hydrogen positions *only* using forcefield methods, before undertaking the full electronic and geometry minimisation. The symmetry of each of the structures was reduced to that of *P*1, and the lattice parameters were allowed to independently vary under geometry optimisation. We performed two geometry-optimisation calculations on each phase, one in which the extra-framework water was present and one in which the water was removed. The energy differences between the two phases, with and without water, was found to be less than 0.001 eV (taking the self-energy of water into account), and hence we omitted the extra-framework water from further calculations to save additional computational expense.

Hypothetical structures were also generated from the observed structures by translating alternate inorganic layers by half a unit cell to form structures in which the corrugated inorganic layers were either aligned or unaligned relative to each other, as shown schematically in Figure 1. These hypothetical structures were generated to establish the energy difference between the aligned and unaligned phases for each organic chain length to resolve whether thermodynamic or kinetic effects are responsible for directing the formation of one phase over another.

The carbon and hydrogen atoms of the diphosphonate linkers in these hypothetical structures were assigned an appropriate starting position and their positions were subsequently optimised by means of the universal forcefield within the Cerius^2 software (all other atoms and lattice parameters were held fixed).[27] A short (20 ps) molecular dynamics run was performed on the configuration whilst other framework atomic positions were held fixed and the system was re-optimised. This process provides a low energy configuration prior to performing the relatively computationally demanding DFT calculations. The initial starting structures of the aluminium butylenediphosphonate structures ($n = 4$) were created from the analogous propylenediphosphonate structures by increasing the inorganic layer separation by 1.205 Å, a value determined from the average increase in layer separation between the optimised structures of ethylenediphosphonate and propylenediphosphonate. The starting positions of the carbon and hydrogen atoms were generated in the manner described previously.

All the structures produced were relaxed at constant pressure and 0 K to determine the total lattice energy for each structure. During the optimisation, all atomic degrees of freedom were allowed to vary and the lattice parameters were also free to change to reduce the residual force on each atom to approximately zero.

To assess whether the energy differences between the aligned and unaligned structures of the aluminium ethylene- and propylenediphosphonates could be attributed to the chemically distinct organic and inorganic parts of the cell, each final optimised structure was deconstructed to ascertain the contribution to the total energy. The first deconstruction involved removing the organic linkers from the structures to determine the absolute energetic contribution of the inorganic layers to the total energy of the structure. The second deconstruction involved the removal of the inorganic layers to leave only the organic linker groups and the determination of their contribution to the final energy of the structure. The final deconstruction involved removing only one inorganic layer from each unit cell of a complete structure to enable the contribution of any non-direct bonding interactions between the organic linker and the inorganic layers and the P–C bond to the total energy of the complete structure along with the non-bonding interaction between the water and the cell constituents to be determined. A cartoon of the deconstruction process is shown in Figure 4. For each deconstruction, undersaturated atoms within the structure were capped with terminal H atoms to yield fragments with reasonable electronic configurations. The positions of all atoms were fixed and the positions of the capping H atoms on the structural fragments were geometry optimised, firstly by means of the universal force-field, and secondly by means of the first-principles approach using CASTEP.[26]

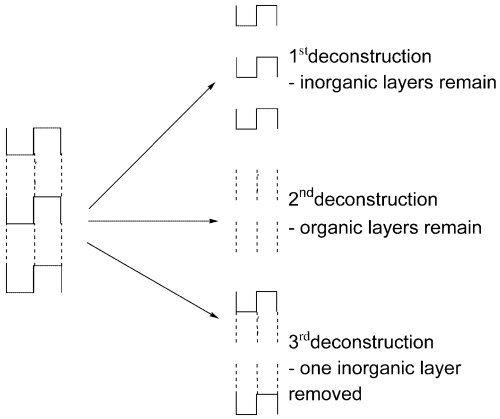

Figure 4. A schematic representation of the chemically distinct parts of an optimised structure formed by the deconstruction process used in this work to ascertain the contribution to the total energy of the optimised structure from each part.

The total energy difference between two phases containing the same diphosphonate moiety (at an effective temperature of 0 K) is computed. We equate this with strain energy, or the minimum energy required to form the hypothetical phase. Of course, other more complex stacking may be possible or energetically accessible; however, since the observed aluminium ethylene- and propylenediphosphonate phases show two possible stacking arrangements, we concentrate on these sequences only.

Results and Discussion

NMR spectroscopy of $Al_2[O_3PC_3H_6PO_3](H_2O)_2F_2{\cdot}H_2O$: The ^{31}P and ^{19}F solid-state MAS NMR spectra of $Al_2[O_3PC_3H_6PO_3](H_2O)_2F_2{\cdot}H_2O$ both contain a single peak at $\delta = 18.15$ and at -139.05 ppm in the ^{31}P and ^{19}F NMR spectra, respectively (see the Supporting Information). Both values are similar to those observed for $Al_2[O_3PC_2H_4PO_3](H_2O)_2F_2{\cdot}H_2O$.[15,16] The observation of a single peak in both spectra supports the theory that the structure has *Pmmn*, and not $P22_12_1$, symmetry. The ^{19}F NMR spectra and the observation of a peak corresponding to fluorine in the EDXA spectrum of the material are in agreement with the assignation of F1 as a fluorine atom within the structure.

Crystal structure of $Al_2[O_3PC_3H_6PO_3](H_2O)_2F_2{\cdot}H_2O$: The full structure of $Al_2[O_3PC_3H_6PO_3](H_2O)_2F_2{\cdot}H_2O$ is shown in Figure 5. The structure is formed from corrugated chains of corner-sharing AlO_4F_2 octahedra running parallel to the *a* axis. These chains contain two types of AlO_4F_2 octahedra: the first type contains an aluminium (Al1) coordinated to two fluorine atoms (F1) in a *trans* configuration with the other corners of the octahedron being occupied by four equatorially arranged oxygen atoms (O1 and O3), which originate from four different diphosphonate groups. The second octahedron consists of a central aluminium atom (Al2), bound to the two fluorine atoms (F1) in a *cis* fashion with the other two equatorial positions being occupied by two diphosphonate oxygen atoms (O2). The axial positions of this AlO_4F_2 octahedron are filled by two co-ordinated water molecules (O4 and O5). The diphosphonate groups link the chains together along the *c* axis through Al–O–P–O–Al bridges and along the [010] direction through the propylene groups to form a three-dimensional framework structure with channels running along the *c* axis. The composition of these Al–O–P layers is identical to those found in $Al_2[O_3PC_2H_4PO_3](H_2O)_2F_2{\cdot}H_2O$.[15] However, the linkage of the inorganic layers differs to that of $Al_2[O_3PC_2H_4PO_3]$-

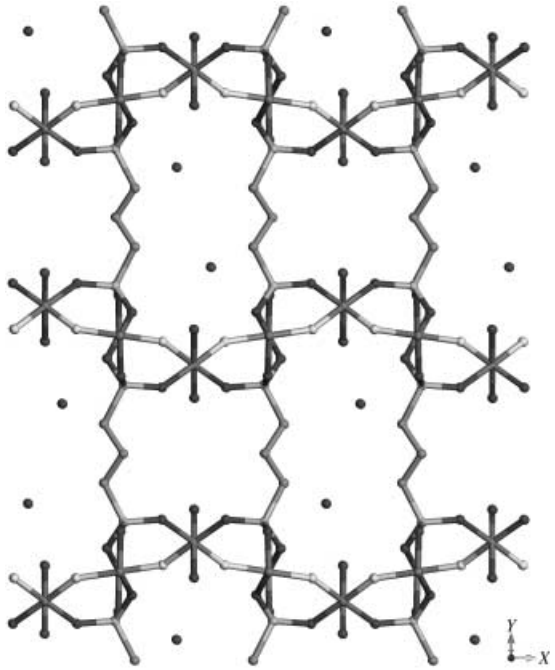

Figure 5. A ball-and stick-representation of the structure of $Al_2[O_3PC_3H_6PO_3](H_2O)_2F_2{\cdot}H_2O$ viewed along the *c* axis. The atom representations ordered from dark to light are: O, Al, C, P, F. Hydrogen atoms are omitted for clarity.

$(H_2O)_2F_2{\cdot}H_2O$, and results in the formation of two types of channel running parallel to the *c* direction. These channels differ in size, shape and composition, as shown in Figure 5. The smaller channel has dimensions 5.729 Å (C2–C2) by 4.527 Å (O5–O5) and is unoccupied. The larger channel is more elongated and measures 4.786 Å (C1–C1) by 9.094 Å (O4–O4). Each large channel contains two extra-framework water molecules (O6) per unit cell. There are eight possible symmetry-related positions that the extra-framework water molecules can occupy; however, only one of each pair of positions at the extremes of each channel is occupied to avoid chemically unreasonable close contacts (Figure 5). The extra-framework water molecules have little interaction with the framework $H_2O(4)$ water molecules which protrude into the pore space (O6–O4 3.409 Å). All the bond lengths and angles found in this structure are similar to those found in $Al_2[O_3PC_2H_4PO_3](H_2O)_2F_2{\cdot}H_2O$ and other related materials.[15,16,28]

Thermal analysis of $Al_2[O_3PC_3H_6PO_3](H_2O)_2F_2{\cdot}H_2O$: The thermogravimetric data for $Al_2[O_3PC_3H_6PO_3](H_2O)_2F_2{\cdot}H_2O$ is shown in Figure 6. The first mass loss of 1.38%, between 30 and 70 °C is corresponds to the loss of surface-bound

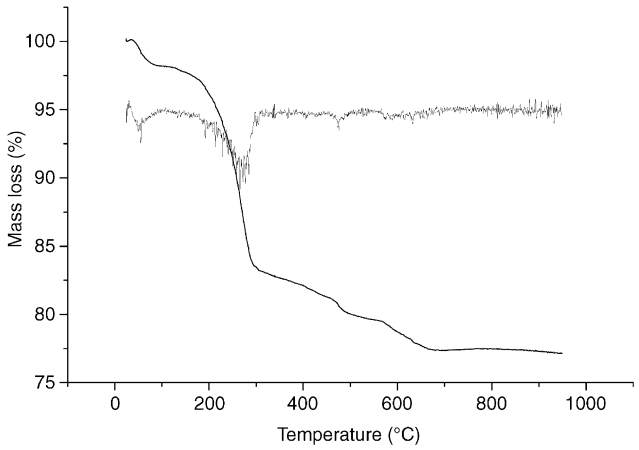

Figure 6. The TGA (black) and first derivative curves (grey) for $Al_2[O_3PC_3H_6PO_3](H_2O)_2F_2{\cdot}H_2O$.

water. The second mass loss of 14.86%, measured between 130 and 310 °C, corresponds to the loss of all three water molecules (calculated 15.60%). The first derivative of the mass-loss curve does not clearly distinguish between the removal of the extra-framework water (O6) and the loss of the framework waters (O4/5). A slower mass loss occurs between 300 and 700 °C, with more rapid, smaller, losses centred at 480 and 610 °C. These losses correspond to the degradation of the organic components and loss of fluoride from the system. However, the observed mass loss in this range, 5.78%, is less than that calculated for the total loss of the organic components, 14.38%, which indicates that the organic components do not fully decompose and are not completely removed.

Structure and energetics of $Al_2[O_3PC_nH_{2n}PO_3](H_2O)_2F_2{\cdot}H_2O$, $n = 2$–4: As mentioned earlier, $Al_2[O_2PC_3H_6PO_3](H_2O)_2F_2{\cdot}H_2O$ and $Al_2[O_2PC_2H_4PO_3](H_2O)_2F_2{\cdot}H_2O$ are composed of isostructural corrugated inorganic Al–O–P sheets. It is the alternating *cis–trans* bridging fluorine atoms that link the octahedra along a constituent chain that result in the sheets adopting corrugations, as observed in Figure 5. These sheets are connected by the alkylenediphosphonate pillars in different configurations to form materials of different topologies. $Al_2[O_3PC_2H_4PO_3](H_2O)_2F_2{\cdot}H_2O$ is composed of inorganic sheets in which the corrugations are aligned and the resultant pores are all alike, as shown in Figure 7a.

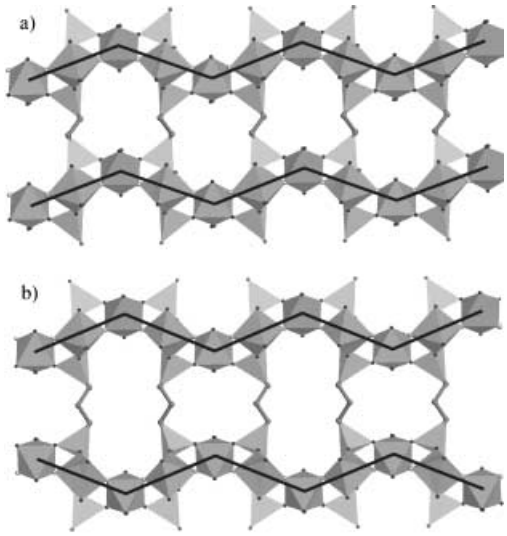

Figure 7. A polyhedral/ball-and-stick representation of the structures of a) $Al_2[O_3PC_2H_4PO_3](H_2O)_2F_2{\cdot}H_2O$ viewed along the *a* axis, and b) $Al_2[O_3PC_3H_6PO_3](H_2O)_2F_2{\cdot}H_2O$ viewed along the *c* axis. The black lines through the Al-centred octahedra highlight the corrugated nature of the layers of polyhedra.

$Al_2[O_2PC_3H_6PO_3](H_2O)_2F_2{\cdot}H_2O$ is composed of unaligned corrugations that result in the formation of two differently sized and shaped channels, as shown in Figure 7b.

The final optimised structures of the aluminium ethylene-, propylene- and butylenediphosphonates are shown in Figure 8. The relative energies of formation for the aluminium ethylene-, propylene- and butylenediphosphonate in aligned and unaligned configurations are given in Table 4. The relative energy differences between the portions of the deconstructed aligned and unaligned structures of the same organic chain length are summarised in Table 4.

The optimised structures of the aligned aluminium ethylenediphosphonate and unaligned aluminium propylenediphosphonate structures are in excellent agreement with the experimental structures. They have the same unit cell parameters (<1% and <2% difference for the aluminium ethylenediphosphonate and propylenediphosphonate structures, respectively) and internal bond lengths and angles within the inherent error of the DFT approach. The range of internal bond lengths and angles for the unaligned aluminium ethylenediphosphonate and aligned aluminium propy-

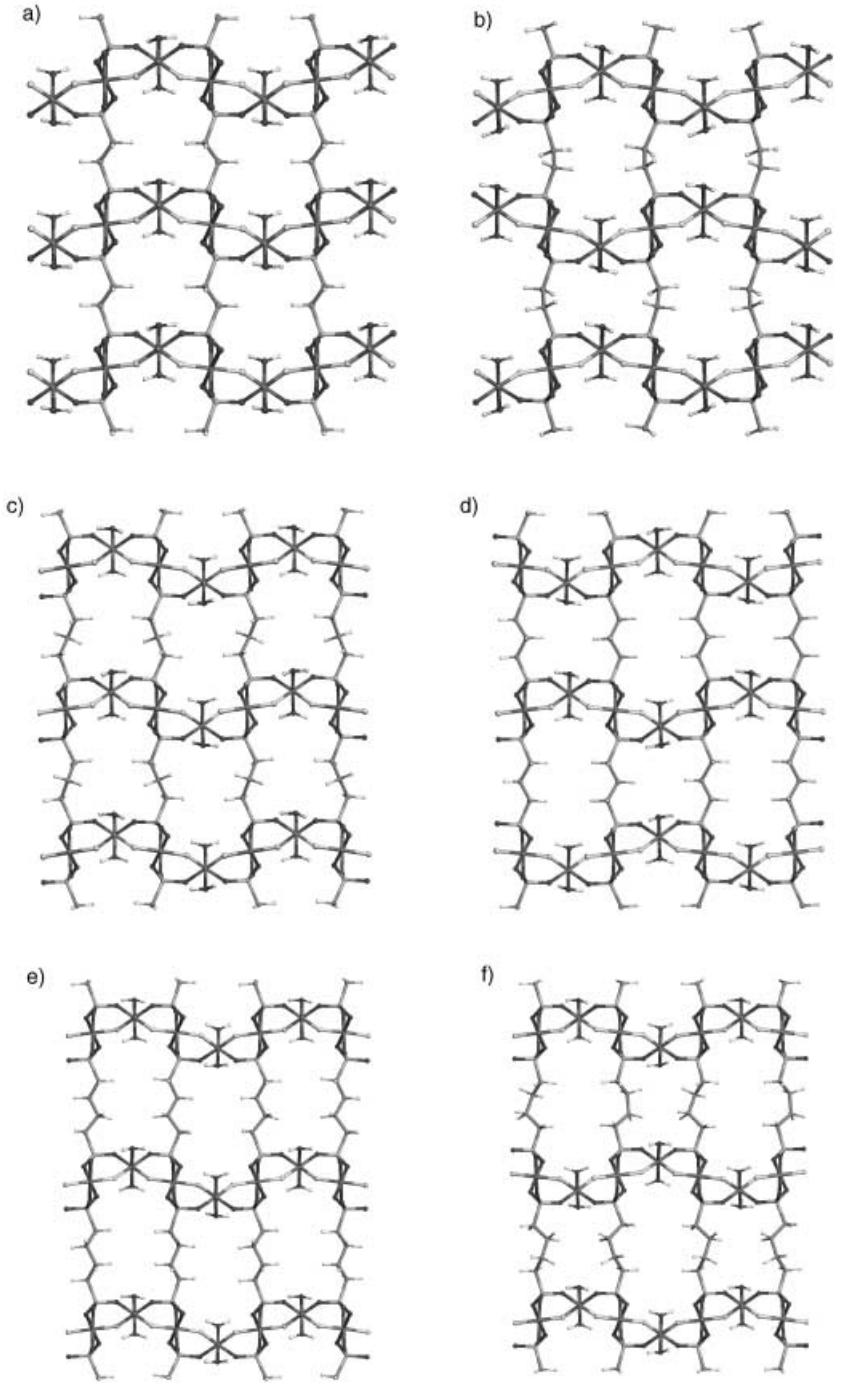

Figure 8. Ball-and-stick representations of the energetically optimised structures of the a) aligned aluminium ethylenediphosphonate, b) unaligned aluminium ethylenediphosphonate, c) aligned aluminium propylenediphosphonate, d) unaligned aluminium propylenediphosphonate, e) aligned aluminium butylenediphosphonate and f) unaligned aluminium butylenediphosphonate materials.

lenediphosphonate structure are consistent with the range expected for these materials.

Reassuringly, the most energetically favourable structures of the aluminium ethylenediphosphonate and propylenediphosphonate pairs of materials are those that are observed experimentally, which indicates that thermodynamics is the primary factor in dictating which stacking arrangement is formed. For the pair of aluminium ethylenediphosphonate structures, the energy of the aligned structure (Figure 8a) is $-111.69\ kJ\,mol^{-1}$ lower than the energy of the unaligned structure (Figure 8b). Consideration of the contributions from the comparable fragments of each structure (see Table 4) shows that the main contribution to this energy difference is from the organic linkers in the aligned and unaligned structure ($-94.25\ kJ\,mol^{-1}$) that arises from the more "strained" organic linker in the latter. The strain induced upon creating the hypothetical structure is dissipated by expanding the C–C and C–P bond lengths and increasing X–C–Y (where X = H, C or P and Y = H or C) angular ranges for the organic fragments of the unaligned aluminium ethylenediphosphonate with respect to the aligned structure, which have values of 1.530–1.533 Å, 1.794–1.812 Å, 103.08–120.42° and 1.524–1.530 Å, 1.782–1.797 Å, 105.73–115.83°, respectively. Significantly, the organic linker in the observed structure has the configuration expected for the ground state of the alkane molecule in vacuo. It is clear that the energy difference between the observed and hypothetical structures is dominated by the difference in energy between the organic linker in the two configurations. A relatively small component of the strain energy is attributed to the stacking of the inorganic layers ($-6.49\ kJ\,mol^{-1}$). Additional minor contributions to the energy difference between phases arise from the strength of the P–C bonds and the nonbonded energy within the cell ($-9.98\ kJ\,mol^{-1}$). Summation of these contributions within the cell gives a total energy difference ($-110.72\ kJ\,mol^{-1}$) that is very close to the difference between the enthalpies of formation between the two phases ($-111.69\ kJ\,mol^{-1}$). This very good agreement indicates that we have accounted for the major energetic contributions to the total energy.

The unaligned aluminium propylene structure (Figure 8d) is more stable than the aligned structure (Figure 8c) by

Table 4. Relative energies of the whole structures, and their respective fragments from the deconstructed structures, of the aligned and unaligned aluminium alkylenediphosphonates.

Structure	Deconstructed structure				
	$\Delta E_{formation}$ [kJ mol^{-1}]	$\Delta E_{inorganic\ layers}$ [kJ mol^{-1}]	$\Delta E_{organic\ linker}$ [kJ mol^{-1}]	$\Delta E_{other\ (P\text{-}C,H\text{-}H)}$ [kJ mol^{-1}]	ΔE_{total} [kJ mol^{-1}]
ethylenediphosphonate, aligned–unaligned, (Figure 8a,b)	−111.69	−6.49	−94.25	−9.98	−110.72
propylenediphosphonate, unaligned–aligned, (Figure 8d,c)	−76.55	+0.15	−84.83	+6.59	−78.09
butylenediphosphonate, aligned–unaligned, (Figure 8e,f)	−48.76	–	–	–	–

−76.6 kJ mol^{-1}. Again, from considerations of the contributions from the comparable fragments of each structure (see Table 4), it can be seen that the main contribution to this energy difference is from the organic linker in the unaligned and aligned structures (−84.83 kJ mol^{-1}). Note that energy difference between the inorganic layers is smaller compared to the aluminium ethylenediphosphonate case; from this we reason that, as the layers are forced apart, the non-bonded interaction decays to zero, and this plays little part in dictating which configuration is formed. Again, we find the total energy difference between the two phases can be found by adding the constituent energy differences. This also indicates that we have accounted for the major energetic contributions to the total energy.

It thus seems apparent that the adoption of an aligned or unaligned arrangement of the inorganic layers in this system, manifested by the total energies of the structures, is dependent on the conformation adopted by the simple alkyl linker to link the relatively inflexible inorganic layers. It is also apparent that alkyl chains with an even number of C atoms give rise to an aligned inorganic layer arrangement, whereas alkyl chains with an odd number of C atoms favour an unaligned layer arrangement. Hence, through the choice of the length of the organic linker, the arrangement of the inorganic layers can be controlled so that a structure with one or two types of channels can be rationally designed. We believe that this rationale extends to the aluminium butylenediphosphonate structures for which the total energy of the aligned aluminium butylenediphosphonate structure (Figure 8e) is −48.76 kJ mol^{-1} lower than the total energy of the unaligned aluminium butylenediphosphonate structure (Figure 8f). Although this material has yet to be synthesised, we predict that the butylenediphosphonate will have an aligned stacking arrangement of the inorganic layers. We hope to report our investigation into the synthesis of this material in due course.

It is noticeable that the relative energy difference between the pairs of aluminium ethylene-, propylene- and butylenediphosphonate structures decreases as the organic linker becomes longer. This may be explained by considering that, as the length of the organic linker increases, there are a larger number of degrees of conformational freedom in the longer chain, and additionally, the strain energy that separates the aligned and unaligned phases can be delocalised or absorbed over more bonds within a longer chain. Given that the strain energy attenuates as a function of the chain length, one might expect, solely on energetic grounds, that when the organic chain length reaches a certain length (when the strain energy is less or approximately equal to kT), aligned and unaligned inorganic layers might occur in the same structure forming an intergrowth structure or a multi-domain phase. Alternatively, co-precipitation of the two phases might produce pure structures with a differing number of channel types.

Conclusion

We have described the synthesis and crystal structure of the hybrid framework material $Al_2[O_3PC_3H_6PO_3](H_2O)_2F_2{\cdot}H_2O$, a member of the $Al_2[O_3PC_nH_{2n}PO_3](H_2O)_2F_2{\cdot}H_2O$ series for which the $n = 2,3$ members are now known. These materials contain isostructural corrugated inorganic Al–O–P layers whose stacking arrangement, either AAAAAA or ABABAB, is dependent upon the configuration and number of C atoms in the alkyl chains linking the inorganic layers. An arrangement of aligned inorganic layers (AAAAAA) produces a structure containing one type of channel, and the arrangement of unaligned inorganic layers (ABABAB) produces a structure containing two types of channel. Our results show that the layer alignment adopted is that for which the organic linker can adopt its most favoured configuration and so the form of the organic linkers controls whether a structure with one or types of channel results. This type of linkage of corrugated inorganic layers by simple organic alkyl chains provides a potent element to the rational design of the micropore volume within hybrid framework materials. Such control over the structure of the micropore volume will prove invaluable in the engineering of new compounds for the numerous applications of microporous materials.

Acknowledgement

The authors would like to thank Dr. A. Aliev, Dr. M. Odhlaya (ULIRS) and Dr. A. Beard (UCL Geology) for help in the collection of the NMR, TGA and EDAX data, respectively. MPA would like to thank the Royal Society for provision of a University Research Fellowship. HGH would like to thank the EPSRC for provision of a quota award and for funding. We thank Accelrys for providing access to the Materials Studio and Cerius^2 software.

[1] C. Janiak, *J. Chem. Soc. Dalton Trans.* **2003**, 2781–2804.
[2] S. L. James, *Chem. Soc. Rev.* **2003**, *32*, 276–288.

[3] H. Li, M. Eddaoudi, M. O'Keeffe, O. M. Yaghi, *Nature* **1999**, *402*, 276–279.
[4] M. Eddaoudi, J. Kim, N. Rosi, D. Vodak, J. Wachter, M. O'Keeffe, O. M. Yaghi, *Science* **2002**, *295*, 469–472.
[5] V. Kiritsis, A. Michaelides, S. Skoulika, S. Golhen, L. Ouahab, *Inorg. Chem.* **1998**, *37*, 3407–3410.
[6] C. Livage, C. Egger, M. Nogues, G. Ferey, *C. R. Acad. Sci. Ser. IIc* **2001**, *4*, 221–226.
[7] F. Serpaggi, G. Ferey, *Microporous Mesoporous Mater.* **1999**, *32*, 311–318.
[8] F. Serpaggi, G. Ferey, *J. Mater. Chem.* **1998**, *8*, 2737–2741.
[9] F. Serpaggi, G. Ferey, *J. Mater. Chem.* **1998**, *8*, 2749–2755.
[10] D. M. Poojary, B. Zhang, A. Clearfield, *J. Am. Chem. Soc.* **1997**, *119*, 12550–12559.
[11] D. I Arnold, X. Ouyang, A. Clearfield, *Chem. Mater.* **2002**, *14*, 2020–2027.
[12] D. M. Poojary, B. Zhang, A. Clearfield, *Chem. Mater.* **1999**, *11*, 421–426.
[13] A. Burton, R. J. Accardi, R. F. Lobo, M. Falcioni, M. W. Deem, *Chem. Mater.* **2000**, *12*, 2936–2942.
[14] H. G. Harvey, M. P. Attfield, *Chem. Mater.* **2004**, *16*, 199–209.
[15] H. G. Harvey, S. J. Teat, M. P. Attfield, *J. Mater. Chem.* **2000**, *10*, 2632–2633.
[16] H. G. Harvey, J. Hu, M. P. Attfield, *Chem. Mater.* **2003**, *15*, 179–188.
[17] M. P. Attfield, H. G. Harvey, B. Slater in *Frontiers of Solid State Chemistry* (Eds.: S. H. Feng, J. S. Chen), World Scientific Publishing, Singapore, **2002**, pp. 177–183.
[18] R. Shirley, D. Louer, *Acta Crystallogr.* **1978**, *A34*, S382.
[19] R. Shirley, *The CRYSFIRE System for Automatic Powder Indexing: User's Manual*, The Lattice Press, Guildford, **1999**.
[20] A. Le Bail, H. Duroy, J. Fourquet, *Mater. Res. Bull.* **1988**, *23*, 447–452.
[21] R. B. Von Dreele, A. C. Larson, GSAS, General Structure Analysis System, Regents of the University of California: LANSCE, Los Alamos National Laboratory, **1995**.
[22] A. Altomare, M. C. Burla, M. Camalli, G. Cascarano, C. Giacovazzo, A. Guagliardi, A. G. G. Moliterni, G. Polidori, R. Spagna, SIRPOW97, Istituto di Ricerca per lo Sviluppo di Metodologie Cristallografiche (IRMEC), Bari (Italy), **1997**.
[23] A. Altomare, M. C. Burla, M. Camalli, B. Carrozzini, G. Cascarano, C. Giacovazzo, A. Guagliardi, A. G. G. Moliterni, G. Polidori, R. Rizzi, *J. Appl. Crystallogr.* **1999**, *32*, 339–340.
[24] A. L. Spek, PLATON, Utrecht University, Utrecht (The Netherlands), **2001**.
[25] J. P. Perdew, K. Burke, Y. Wang, *Phys. Rev. B* **1996**, 54, 16533–16539.
[26] M. C. Payne, M. P. Teter, D. C. Allan, T. A. Arias, J. D. Joannopoulos, *Rev. Mod. Phys.* **1992**, *64*, 1045–1097.
[27] Cerius^2, version 4.2, Accelrys (www.accelrys.com).
[28] N. Simon, N. Guillou, T. Loiseau, F. Taulelle, G. Ferey, *J. Solid State Chem.* **1999**, *147*, 92–98.

Received: January 23, 2004

Published online: May 6, 2004

